Evaluation of x-ray reflectors by optical diffraction patterns

Takayuki Hayashi, Takashi Okajima, Yang Soong

Takayuki Hayashi, Takashi Okajima, Yang Soong, "Evaluation of x-ray reflectors by optical diffraction patterns," Proc. SPIE 10699, Space Telescopes and Instrumentation 2018: Ultraviolet to Gamma Ray, 106993X (6 July 2018); doi: 10.1117/12.2310018

SPIE.

Event: SPIE Astronomical Telescopes + Instrumentation, 2018, Austin, Texas, United States

Evaluation of x-ray reflectors by optical diffraction patterns

Takayuki Hayashi[a,b], Takashi Okajima[a], and Yang Soong[a,b]

[a]NASA's Goddard Space Flight Center, Greenbelt, MD 20771 USA
[b]University of Maryland, Baltimore County, 1000 Hilltop Cir, Baltimore, MD 21250 USA

ABSTRACT

Performance of X-ray reflectors affects that of X-ray mirrors. Modern X-ray mirrors have thousands of reflectors to gain large effective area. Evaluation of the reflectors is an important process in production of the mirrors. A diffraction pattern dominates reflector image when the parallel optical beam illuminates the reflector along its optical axis because the reflectors are used at grazing incident angles of around 1 deg and their effective width are 1–10 mm. A diffraction pattern from the entire reflector surface can be acquired at once with the aid of a lens. The diffraction pattern holds information of the surface profiles of the reflectors. To quantitatively evaluate the reflectors with the diffraction pattern, we created a diffraction pattern model by the wave optics with the ideal surface profile and fitted it to data. As a result, a correlation between fitting residual and the normal vector distribution of the surface profile was found. With our method, the reflectors can be evaluated and sorted out more efficiently.

Keywords: X-ray mirror, X-ray reflector, ASTRO-H, X-ray Astronomy Recover Mission (XARM), Optical diffraction, Manuscript format, Fraunhofer diffraction, Reflector mass production

1. INTRODUCTION

Since the refraction index for X-rays is slightly less than 1, the total external reflection occurs at a grazing incidence angle of around 1 deg. In most cases, the total external reflection is used for X-ray optics. In particular, X-rays from celestial objects are focused with X-ray mirrors of Wolter-I type optics in general. The Wolter-I type X-ray optics is made of paraboloid and hyperboloid and, incident X-rays are reflected once by the paraboloid and once by the hyperboloid and, focused at the focal point. Width of the photon passage of the reflectors is typically 1–10 mm, which is narrower than the generating length of the reflectors by two orders of magnitudes. Therefore, a diffraction patterns dominates the imaging process when the parallel optical beam illuminates the reflectors from their optical axes. We may be able to estimate surface profile of the reflectors with the diffraction patterns because the diffraction patterns vary with the underlying surface geometrical structures of the reflectors. The diffraction patterns of not only one generating line on the reflector but also every line at any location on the surface can be acquired at once with a simple and inexpensive setup (see § 2). As a matter of course, the reflector surface profile crucially affects total performance of the X-ray mirrors.

Modern X-ray mirrors have thousands of reflectors and evaluation of the reflector is an important process in production of the X-ray mirrors. As mentioned above, since the X-ray reflectors are grazing incident optics, the effective area of a single reflector is small. Therefore, the effective area of the X-ray mirrors is increased by nesting a number of the reflectors. For example, one of the Soft X-ray Mirror (SXT) of ASTRO-H (left of figure 1) had 1624 reflectors (right of figure 1). The SXT reflectors were designed as conical shells azimuthally divided into four pieces to simplify their fabrication. Their generating length is 101.6 mm. To enhance the mirror performance, efficient selection of reflectors is crucial in their mass production within limited time.

We developed a reflector evaluation method using the optical diffraction patterns. First, an optical measurement system was constructed to acquire the diffraction pattern of the reflector as described in § 2. To extract information of the reflector profile, we created a diffraction pattern model by the wave optics and presented the modeling in § 3 in brief. The model was applied to the diffraction data of the SXT reflectors as shown in § 4. As a result, we found a correlation between residual of the model fitting and the reflector profile measured by a well-established displacement sensor. In § 5, we summarize our reflector evaluation method.

Further author information: (Send correspondence to Takayuki Hayashi)
Takayuki Hayashi: E-mail: takayuki.hayashi@nasa.gov, Telephone: +1 (301) 286-2454

Space Telescopes and Instrumentation 2018: Ultraviolet to Gamma Ray, edited by Jan-Willem A. den Herder, Shouleh Nikzad, Kazuhiro Nakazawa, Proc. of SPIE Vol. 10699, 106993X · © 2018 SPIE
CCC code: 0277-786X/18/$18 · doi: 10.1117/12.2310018

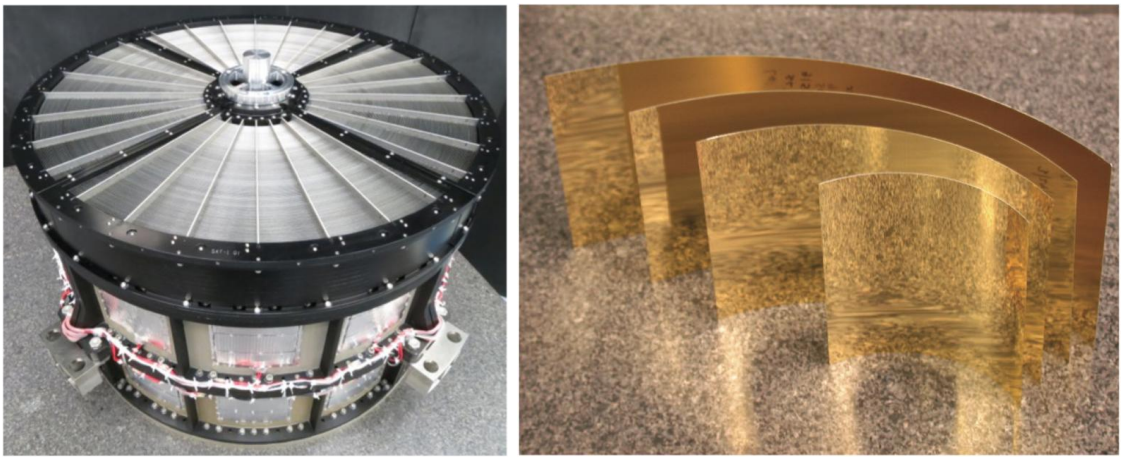

Figure 1. Left: One of the ASTRO-H Soft X-ray Telescopes (SXTs). Right: Reflectors of the SXTs. 1624 reflectors were installed into one module of the SXTs.

2. OPTICAL MEASUREMENT

Figure 2 shows our optical measurement setup. An isotropic source located at the focal point of a parabolic mirror. Isotropic white light is emitted from the source and converted into parallel beam by reflecting by the parabolic mirror after being filtered by a bandpass filter of 675–725 nm. Note that the red wave length is adopted to extend the diffraction pattern. The red parallel beam is reflected upward by a flat mirror and illuminates the reflector standing on a glass plate. The red light reflected by the reflector is reflected again by another flat mirror, goes though a lens and is focused on a CMOS detector at last. The lens and the CMOS camera are integrated. The focal length of the lens is adjustable from 400 mm to 1000 mm. The CMOS camera is NIKON-Df whose number of pixel is 4928×3280 and pixel size is $7.3\times7.3\,\mu\mathrm{m}^2$. The CMOS camera is always located at the focal point of the lens to give us the Fraunhofer diffraction pattern of the light reflected by the reflector. The shape of the Fraunhofer pattern is independent of distance between the reflector and the lens.

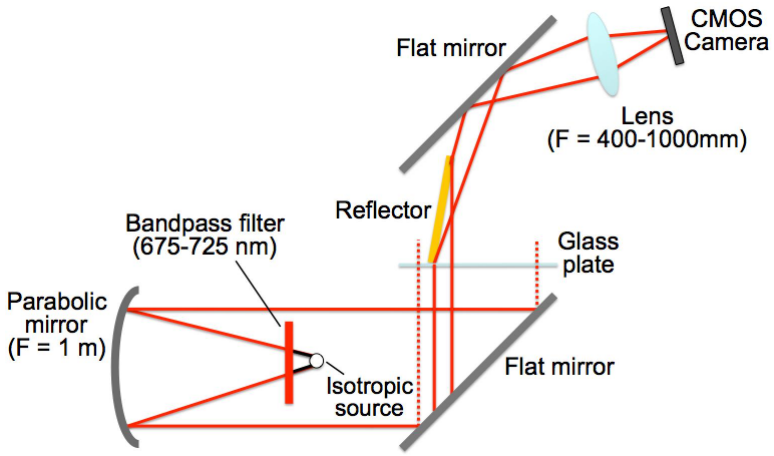

Figure 2. Optical measurement setup.

Figure 3 is a diffraction pattern image of a reflector of the SXT. This image consists of only R pixels to exclude the difference between R, G and B in the sensitivity to the red light. The clear diffraction pattern is seen centering the brightest arc. The length of the arc is attributed to the azimuthal length of the reflector. The pattern varies along the azimuthal direction.

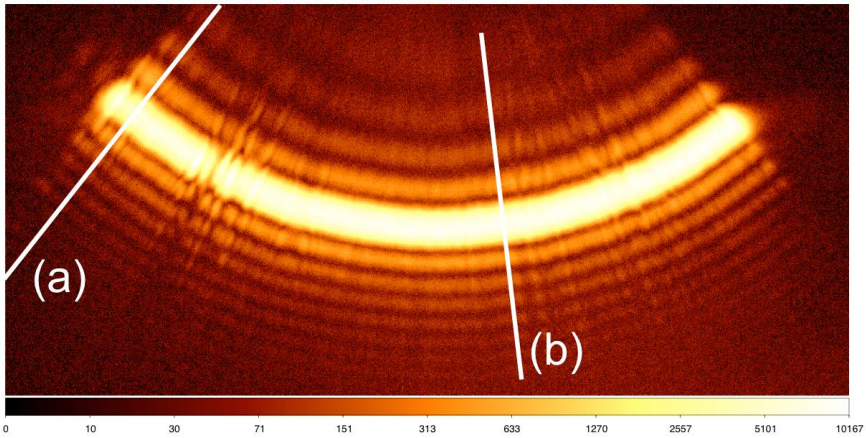

Figure 3. A diffraction pattern image of the reflector. Lines of (a) and (a) show position where diffraction patterns in figure 7 were extracted

3. DIFFRACTION PATTERN MODEL

To quantitatively evaluate the reflectors with their diffraction patterns, we modeled the diffraction pattern with the wave optics. Figure 4 shows a schematic diagram of forming a diffraction pattern. A parallel beam illuminates every point on the reflector and elementary waves are generated at the every point in the order in which the parallel beam arrives. The elementary waves form a new wave front and, in other words, the wave front of the reflection. Next elementary waves are generated when the reflected light arrives at a lens. At this time, the reflection wave front undergoes a conversion which converts parallel beams into a spherical wave focusing at a point focal length away from the lens. Intensity of the image on the lens focal plane can be written as

$$I(x_{\mathrm{D}}) = \int dt \left(\iint dx_{\mathrm{r}} dx_{\mathrm{l}} \exp(\omega t - ik(L_0(x_{\mathrm{r}}, x_{\mathrm{l}}) + L_1(x_{\mathrm{l}}, x_{\mathrm{D}}))) \exp(-if(x_{\mathrm{l}} - F))/(L_0 + L_1) \right)^2, \qquad (1)$$

where $x_{\mathrm{r}}, x_{\mathrm{l}}, x_{\mathrm{D}}$ are positions of points on the reflector, lens and detector, respectively. L_0 and L_1 are distances between x_{r} and x_{l} and, between x_{l} and x_{D}, respectively. ω, k and t are angular frequency, wave number and time, respectively. The term of $\exp(-if(x_{\mathrm{l}} - F))$ expresses the conversion by the lens, where F is the focal length of the lens.

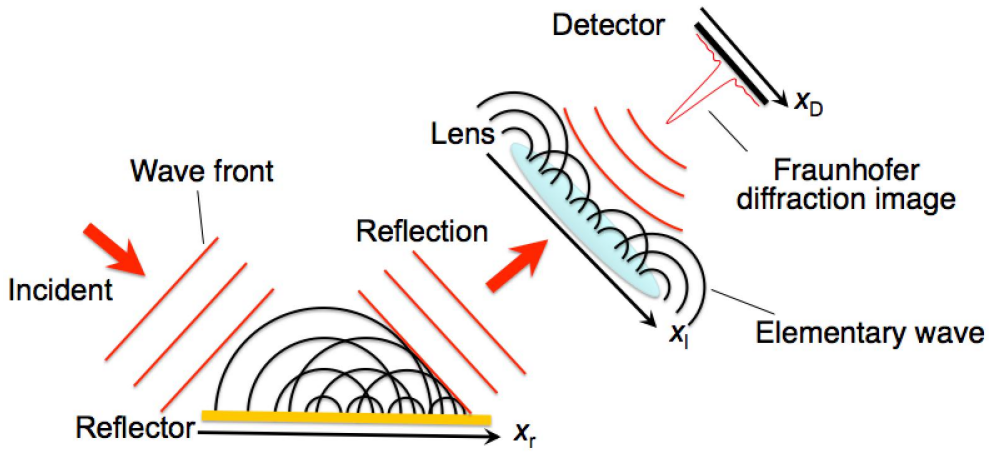

Figure 4. A schematic diagram of forming a Fraunhofer diffraction image.

We obtained theoretical diffraction patterns as shown in figure 5 by numerical calculation. Left and right panels show cases of incident $\theta_{\rm in} = 0.2$ and 1.0 deg, respectively. Since the SXT reflector is conical shell, the reflector surface is assumed to be completely flat in these calculation. The pattern is asymmetric in general unlike that formed by that the parallel beam goes though the slit. Moreover, the asymmetry is more noticeable with smaller incident angle. This is because the elementary waves are not generated from the backside of the reflector. With the smaller incident angle, detector area seeing the backside is larger and this effect becomes more important. The calculation was performed with incident angles at intervals of 0.01 deg between 0.1 and 2.2 deg which covers all of cone angles of the SXT reflector. The calculated diffraction pattern was compiled into the XPSEC software with a free parameter of the incident angle as a table model to fit to data (XPSEC is a well-established astronomical X-ray spectral fitting tool).

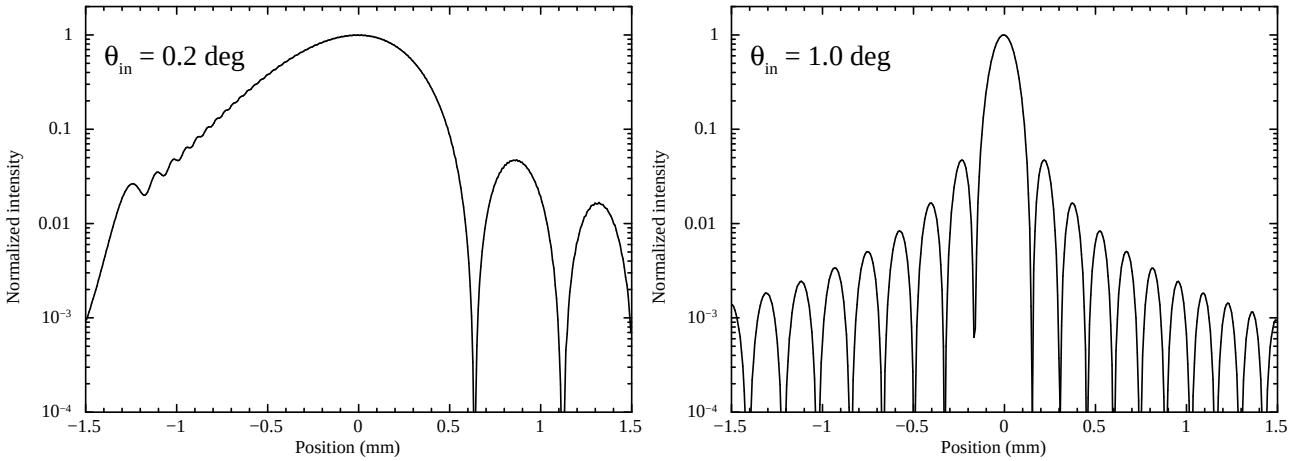

Figure 5. Calculated diffraction pattern of $\theta_{\rm in} = 0.2$ deg (left) and 1.0 deg (right). The focal length of the lens is assumed to be 400 mm. Intensities are normalized by the maximums of each pattern.

To verify the model, the model was fitted to diffraction patterns of an optical flat whose surface can be considered to be completely flat. The optical flat was illuminated by the red parallel beam in the same manner as the reflector in §2. The length of the optical flat is 100 mm similar to the SXT reflectors. Figure 6 shows an intensity profile of a diffraction pattern of the optical flat with black crosses. The model was fitted to the diffraction pattern by thawing the parameter of the incident angle and a width of a Gaussian function to convolve the diffraction pattern model. The Gaussian function was introduced because the parallel beam is not perfect mainly because of a finite size of the isotropic point source (see figure 2). Red line overlapped with data points is the best-fitted model and the bottom panel shows the residual between the data and the model, which indicates the model reproduces the data very well. Moreover, a part of the diffraction pattern close to the edge of $+x_{\rm r}$ in figure 4 (i.e. left part of the diffraction patterns in figure 5 and 6) was excluded in the fitting because this part is too sensitive to the incident angle and easily contaminated by direct incident of the parallel beam. In the case of figure 6, the incident angle was measured to be $\theta_{\rm in}$=0.54 deg.

4. MODEL APPLICATION

The model was fitted to the diffraction patterns of the SXT reflectors. Left (a) and right (b) panels of figure 7 show intensity profiles along lines of (a) and (b) in figure 3, respectively. The red lines are best-fitted models for each and bottom panels show residuals. The fitting was performed in the same manner as the optical flat except the convolution. The Gaussian function to convolve was that determined by the fitting to the optical flat. Apparently, the fitting of (b) is better than that of (a). In fact, the reduced-χ^2 of (b) is ~ 4.1 and better than that of (a) ~ 48.1 by one order of magnitude, which implies that the reflector surface of (b) is flatter than that of (a).

We found a correlation between the reduced-χ^2 and the surface profile of the reflector. We measured surface profiles of several dozens of generating lines on several reflectors by a well-established laser displacement sensor as

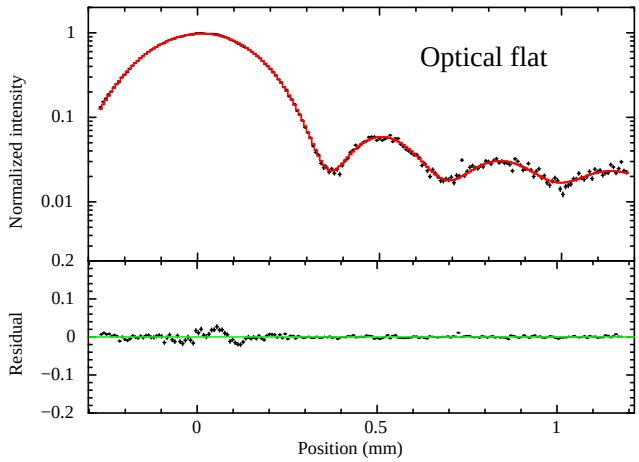

Figure 6. A diffraction pattern of the optical flat (black cross) and the best fitted model (red line). The residual is shown in the bottom panel.

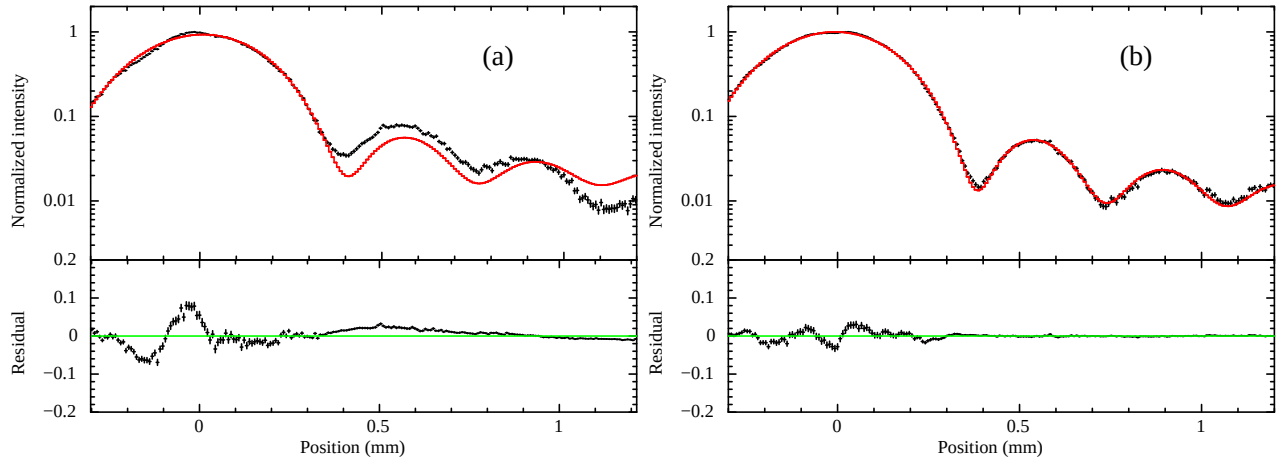

Figure 7. Diffraction patterns of a reflector (black cross) and the best fitted models (red line). Left and right patterns are extracted from line (a) and (b) in figure fig:pattern, respectively. The residuals are shown in the individual bottoms panel.

shown in the left panel of figure 8. Normal vector distribution of the reflectors were calculated from the measured profiles (right of figure 8). A diameter, within which 90 percent of area of the normal vector distribution is enclosed (90 percent power diameter), is an index to represent performance of the reflector profile. A smaller 90 percent power diameter means better imaging performance. Meanwhile, we fitted the model to the diffraction patterns of the dozen reflectors and acquired the reduced-χ^2. Figure 9 shows the correlation between the 90 percent diameter and the reduced-χ^2. This correlation is not strong but we can exclude extremely bad reflectors with this correlation adopting the reduced-χ^2=0.5 as the selection threshold (dotted vertical line in figure 9), for example. We will search for a stronger correlation improving the measurement and analysis.

5. SUMMARY

We developed an X-ray reflector evaluation method using optical diffraction patterns. The seeing width of the reflectors is typically 1–10 mm, and the diffraction patterns are formed when an optical beam illuminates them along their optical axes. The diffraction patterns keep the information of the surface profile of the reflectors and, therefore, can be used for evaluation of the reflectors.

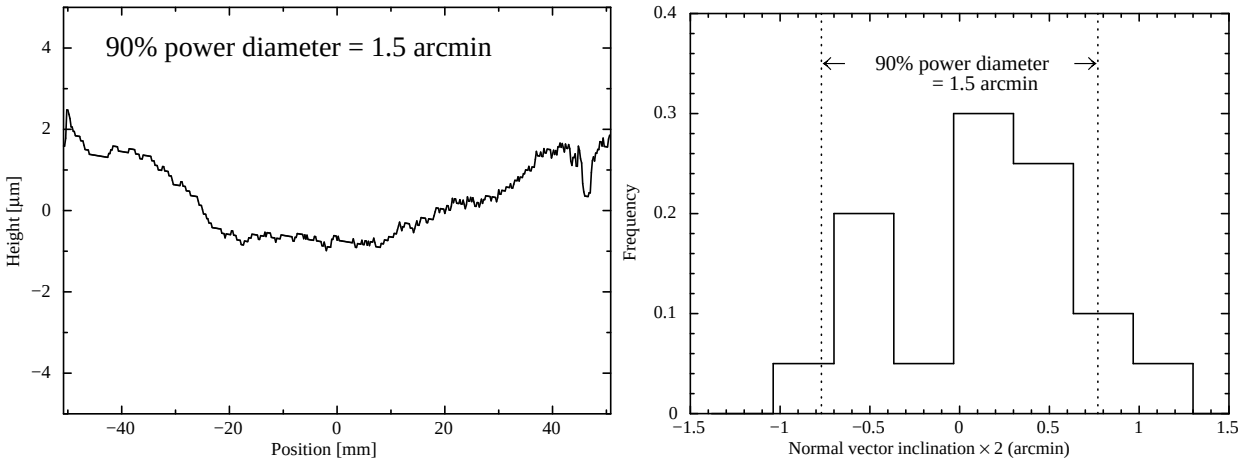

Figure 8. Left: A reflector surface profile measured by the laser displacement sensor. Right: Normal vector distribution of the left profile. The normal vector inclination in the horizontal axis is doubled with consideration for the reflection.

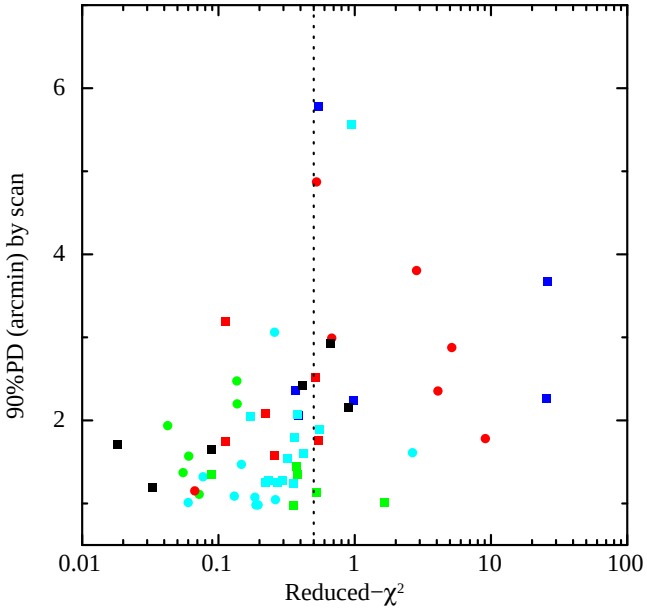

Figure 9. Correlation between the fitting residuals and 90 percent diameter of normal line distribution of the reflectors. Different color or shape show different reflectors. The dotted vertical line shows the reduced-$\chi^2 = 0.5$

The diffraction patterns from the whole reflector are acquired by the CMOS camera at once. The reflector is illuminated by a monochromatic optical parallel beam whose wavelength is 675–725 nm and, the reflected light goes through a lens and forms the Fraunhofer diffraction image on the CMOS camera. The longer wavelength extends the diffraction pattern to easily capture the feature. The shape of the Fraunhofer diffraction is independent of distance between the reflector and the lens.

To extract the information of the reflector profile, we model the diffraction patterns by the wave optics. Elementary waves generated from the reflector surface are integrated on the detector after conversion by lens which converts parallel beams into a spherical wave. The calculated theoretical diffraction pattern is asymmetric because of no elementary wave from backside of the reflector. The model was verified by reproducing the diffraction pattern data of an optical flat very well.

A correlation between reduced-χ^2 of the fitting to reflector data and the reflector profiles was found. Sur-

face profile of several dozens of generating lines on several reflectors were measured by a well-established laser displacement sensor, which gave us the normal vector profile of the reflectors. Meanwhile, the diffraction model was fitted to the several dozen lines and reduced-χ^2 was computed. The reduced-χ^2 correlates with breadth of the normal vector profiles. We can efficiently evaluate the reflectors with the correlation. We will attempt to enhance the correlation and accuracy of the evaluation.

REFERENCES

[1] Okajima, T., et al., "Soft x-ray mirrors onboard the NeXT satellite", *proc. SPIE* **7011**, Space Telescopes and Instrumentation 2008: Ultraviolet to Gamma Ray, 70112X (15 July 2008)

[2] Soong, Y., et al., "ASTRO-H Soft X-ray Telescope (SXT)", *proc. SPIE* **9144**, Space Telescopes and Instrumentation 2014: Ultraviolet to Gamma Ray, 914428 (31 July 2014)

[3] Zhang, W. W., "Manufacture of mirror glass substrates for the NuSTAR mission", *proc. SPIE* **7437**, Optics for EUV, X-Ray, and Gamma-Ray Astronomy IV, 74370N (31 August 2009)